NREL/TP-411-8122 • UC Category: 1262 • DE95009273

Microstructure of Amorphous-Silicon-Based Solar Cell Materials by Small-Angle X-Ray Scattering

Annual Subcontract Report 6 April 1994 – 5 April 1995

D. L. Williamson
Colorado School of Mines
Golden, Colorado

NREL technical monitor: W. Luft

National Renewable Energy Laboratory
1617 Cole Boulevard
Golden, Colorado 80401-3393
A national laboratory of the U.S. Department of Energy
Managed by Midwest Research Institute
for the U.S. Department of Energy
under contract No. DE-AC36-83CH10093

Prepared under Subcontract No. XAN-4-13318-04

August 1995

NOTICE

Available to DOE and DOE contractors from:
Office of Scientific and Technical Information (OSTI)
P.O. Box 62
Oak Ridge, TN 37831
Prices available by calling (615) 576-8401

Available to the public from:
National Technical Information Service (NTIS)
U.S. Department of Commerce
5285 Port Royal Road
Springfield, VA 22161
(703) 487-4650

Printed on paper containing at least 50% wastepaper and 10% postconsumer waste

1. EXECUTIVE SUMMARY

1.1 PREFACE

This report presents results of research performed from April 6, 1994 to April 5, 1995 under a cost-reimbursible subcontract from the National Renewable Energy Laboratory (NREL, a national laboratory of the U.S. Department of Energy operated by Midwest Research Institute) to the Colorado School of Mines (subcontract number XAN-4-13318-04 to the prime contract DE-AC02-83CH10093). The research was carried out under the direction of Don L. Williamson, Professor of Physics. Materials characterization, including small-angle x-ray scattering, x-ray diffraction, and flotation density, were carried out in the Physics Department of the Colorado School of Mines. The materials for analyses were supplied by NREL-supported device-making groups as well as by other groups with relevant expertise. Electron microprobe analyses of film compositions were carried out by Alice Mason of NREL. TEM measurements were made by Kim Jones of NREL. Graduate research assistant Donghoon Min participated in all aspects of the research in pursuit of his M.S. degree in Physics and graduate student Troy Berens contributed to the research.

1.2 OBJECTIVES

The general objective of this research is to provide detailed microstructural information on the amorphous-silicon-based, thin-film materials under development for improved multijunction solar cells. Correlation of this microstructure with opto-electronic properties and device performance is an integral part of the research. The experimental technique used is small-angle x-ray scattering (SAXS) and it provides quantitative microstructural data on microvoid fractions, sizes, shapes, and their preferred orientations. Other microstructural features such as alloy segregation, hydrogen-rich clusters and alloy short-range order are probed. Three types of material are under investigation and fall into the bandgap classification scheme forming the basis of three of the four NREL Amorphous Silicon Teams. Specific objectives in each of the Team areas that were addressed during this first phase were:

(i) Low-bandgap - Develop alternative deposition techniques for high-quality a-SiGe:H alloy materials and devices. Establish correlation of film properties with growth chemistry.

(ii) Mid-bandgap - Investigate the role of large-scale and small-scale microstructure in a-Si:H materials.

(iii) High-bandgap - Develop better high-bandgap materials. Determine the role of ion

bombardment on material quality.

1.3 CONCLUSIONS

1.3.1 Low-Bandgap Material ($a\text{-}Si_{1-x}Ge_x:H$)

The effect of 94% hydrogen dilution versus 0% dilution of silane and germane source gases during PECVD growth for alloys prepared by IACS (Indian Association for the Cultivation of Science) with x up to 0.7 is to reduce the amount of SAXS-detected microstructure and to reduce the degree of preferred orientation. The photoconductivity, $\eta\mu\tau$ product, and Urbach energy are all improved by the hydrogen dilution for $x>0.2$. The results support the concept that the growth chemistry, film microstructure, and opto-electronic properties can be modified by hydrogen dilution.

Use of unusually high hydrogen dilution versus more standard dilution in films with $x\sim0.3$ at USSC yields highly oriented microstructural features about 7 nm in diameter and more than 20 times this dimension in length. These objects could not be detected by TEM. Their orientation parallel to the solar cell transport direction and their relatively low density as determined by SAXS are apparently not detrimental since this material is currently producing the best low-bandgap devices at USSC. Aside from these highly elongated features, the material is otherwise relatively homogeneous in that the nanovoids found in poor-device-quality a-Si:H are not detected.

New alloys on the Ge-rich side ($x>0.5$) prepared at Harvard University have unusually low SAXS-detected microstructure and little preferred orientation. Microvoid volume fractions are below 0.02% in some samples. This was accomplished by more ion bombardment during deposition and suitable hydrogen dilution. The opto-electronic properties are significantly improved compared to earlier results for similar x. The defect density of these materials as determined by drive-level-capacitance at the University of Oregon was found to be unusually low.

Films with $x=1$ (no Si) prepared by sputtering at Kaiserslautern University have extremely low SAXS-detected microstructure and large differences in surface roughness depending on the substrate used. Crystalline Si substrates yield smoother surfaces compared to the Al-foil substrates and microvoid fractions are well below 0.01 vol.%. These results correlate with low Urbach energies (<50 meV).

Analysis of the diffuse SAXS intensity from all the a-SiGe:H alloys studied to date yields no evidence for short-range ordering or clustering on the basis of comparison to the theoretical Laue monotonic scattering prediction.

1.3.2 Mid-Bandgap Material (a-Si:H)

A new absolute intensity calibration of the SAXS system has allowed new determinations of the microvoid densities in a-Si:H films without the need of the earlier flotation density method of void calibration. Results from current device quality a-Si:H prepared by NREL, USSC, Solarex, APS, and IACS show void fractions near the present detection limit of about 0.01 vol.%. Remaining SAXS-detected features can be classified as large-scale structure (≥20 nm). The amount of this structure and its preferred orientation varies remarkably among the samples from the different groups. Surface roughness or residual columnar-like microstructure are the two likely causes. Microvoid fractions in the range of 0.1 to 1 vol.% with very small sizes of the order of 1-2 nm are correlated with poorer device performance.

Hotwire films prepared at NREL under conditions that yield low H contents and improved stability have much lower SAXS intensities than previously studied hotwire material that contained more H. The microvoid density in these new films are comparable to those of the best PECVD a-Si:H. Device studies of the hotwire a-Si:H are underway at NREL.

A series of a-Si:H films prepared under different amounts of Ar dilution by IACS yields improved device-quality behavior and the SAXS is remarkably low for such high Ar dilution (98%) and such high H content (≥18 at.%). Densification of these films relative to those made with no Ar dilution is attributed to bombardment of the growing surface by excited Ar atoms. In contrast, earlier Ar dilution in the VHF-PECVD method at Neuchatel University led to strong SAXS intensities and films with degraded opto-electronic properties.

The effect of ion bombardment during depostion of pure a-Si via magnetron sputtering by the group at University of Illinois is under investigation. Understanding of such effects without H should help improve understanding the behavior when H is added. Clear differences in SAXS-detected microstructures are detected for different ion bombardment conditions.

Unusual deposition conditions explored at Ecole Polytechnique involving either helium dilution or hydrogen dilution has yielded low SAXS-detected microstructures at high depostion rates (1.5 nm/s) or low substrate temperatures (100°C). These a-Si:H films have low defect densities ($\leq 1 \times 10^{16}$ cm^{-3}) and low Urbach energies (≤50 meV).

A systematic study of the hydrogen-related microstructure and its thermal evolution in a-Si:H prepared by ion implantion methods in collaboration with a group in the Netherlands has led to new information on the solubility and clustering of H. Combined SAXS, SIMS, TEM, and IR results show that only about 3 to 4 at.% H is

soluble in this high-purity form of a-Si, that no microvoids are present in the as-implanted state, that H precipitates into nanobubbles beginning at about 350°C if the local H content is near 20 at.%, and that these bubbles are initially only 1 nm in diameter and grow to about 3 nm diameter at 550°C. TEM has imaged these bubbles and confirmed the size determined by SAXS. A sample of pure a-Si containing no H was also shown to contain no detectable microvoids and therefore the known density deficit of 1.8% was established to be due other causes, most likely an average Si-Si bond-length increase of 0.6%. Structural relaxation of the a-Si network due to thermal annealing was observed by decreases in the diffuse SAXS intensity.

1.3.3 High-Bandgap Material ($a\text{-}Si_{1-x}C_x:H$)

Based on the new absolute SAXS intensites, the Solarex a-SiC:H films prepared for study by the High-bandgap Team are all found to contain nanovoid volume fractions of the order of 1% or greater. This fraction is two orders-of-magnitude larger than typical device-quality a-Si:H and occurs even for the smallest additions of carbon (x=0.06). Hydrogen dilution reduces the nanovoid density and improves the opto-electronic properties.

A series of B-doped a-SiC:H alloys prepared by reactive magnetron sputtering at University of Illinois have nanovoid volume fractions that vary from 0.3 to 3.6% depending on hydrogen dilution and carbon content. A maximum optical bandgap (Tauc) of only 1.85 eV was achieved for carbon contents of about 20 at.%. No hydrogen dilution yielded the lowest void fraction and the highest flotation density yet observed for a-SiC:H (2.34 g/cm^3), but the optical gap of this film was only 1.43 eV.

TABLE OF CONTENTS

LIST OF FIGURES

page

LIST OF TABLES

2. INTRODUCTION

Small-angle scattering techniques utilizing x-rays (SAXS), electrons (SAES), or neutrons (SANS) provide rather direct structural information on electron and composition fluctuations in any type of material on a size scale from below one nanometer up to about a hundred nanometers. Since the original applications of small-angle scattering techniques to a-Si [1,2], a-Ge [3,4], and a-Si:H [5-7], several groups have applied these methods to further characterize the nanostructure of a-Si:H [8-13] as well as the important, related alloy systems a-$Si_{1-x}Ge_x$:H [14-16] and a-$Si_{1-x}C_x$:H [11,17,18]. There is one report of a light-induced change in H-related nanostructure of a-Si:H based on SANS [19] and a proposed model [20]. Amorphous-Si-based materials of particular interest for our SAXS research [21] are films being incorporated into current state-of-the-art solar cells and modules along with those under consideration for improved solar cell efficiency and stability. Films with a wide range of compositions, prepared by several film- and device-making groups using various deposition methods and conditions have been examined.

Considerable circumstantial evidence has been acquired suggesting that nanostructure in the form of 1 to 4 nm voids or H-rich clusters is harmful to the opto-electronic properties and device performance [15,16,22-27]. As will be demonstrated in this discussion of our work during the last year, device-quality a-Si:H films prepared by PECVD or hot-filament CVD have nanovoid volume fractions near or below our present detection limit of about 0.01 %. Often the only SAXS signals from a-Si:H (aside from a well-defined diffuse component) are due to some larger-scale features (>30 nm) that are related to surface roughness or residual columnar-like structure. Both a-$Si_{1-x}Ge_x$:H and a-$Si_{1-x}C_x$:H alloy systems exhibit significant increases in heterogeneity with increasing x but the nature of the altered nanostructure is quite distinct for the two systems.

Atomic-scale features such as alloy randomness and static disorder, not studied previously with small-angle techniques for the above materials, have been examined by quantitative studies of the diffuse component of the SAXS. The contributions due to static disorder of the a-Si matrix as well as from the H alloying are clearly identified for a-Si:H.

The next section reviews briefly our present method for interpretation of SAXS data from the materials of interest, including the diffuse scattering contributions. A brief description of the experimental methods, including our new conversion of the SAXS intensities into absolute units (electrons/atom), will be followed by results obtained during the last year with the three classes of materials: a-$Si_{1-x}Ge_x$:H (low-gap), a-Si:H (mid-gap) and a-$Si_{1-x}C_x$:H (high-gap).

3. SAXS INTERPRETATION

The usual orientation in SAXS experiments is to place a sufficiently thin sample (thickness ~ $1/\mu$, where μ is the linear absorption coefficient of the sample for the x-ray energy in use) in transmission geometry such that the momentum transfer vector **q** lies in the plane of the sample. This allows study of electron density fluctuations parallel to **q** with sizes of the order of 1/q. The SAXS intensity is collected over a range of **q** and plotted versus the magnitude $q=(4\pi/\lambda)\sin\theta$, where 2θ is the scattering angle and λ is the x-ray wavelength. Anisotropic scattering due to non-spherical scattering objects that have a preferred orientation in the sample can be revealed with two-dimensional detectors [7] or by tilting the sample in the beam so that **q** no longer lies in the plane of the sample [3]. There are numerous methods of inversion of the SAXS intensity I(**q**) from momentum space to real space to extract structural details of the objects causing the scattering such as their shape, size distribution, preferred orientation, and spatial correlation [28].

To interpret the intensity from our small-angle scattering experiments it is convenient to divide it into three components:

$$I(q) = I_L(q) + I_N(q) + I_D, \tag{1}$$

where we now assume there is no preferred orientation of the scattering objects so that only the magnitude of **q** is needed. $I_L(q)$ represents the intensity from large-scale objects that are so large that their primary scattering occurs well below the lowest angle accessible by the experimental apparatus. Thus only the "tail" of the scattering curve is seen from these large objects and ususally exhibits a well-known power-law dependence (Porod law) in the case that the objects have sharp electron density boundaries, i.e.

$$I_L(q) = Aq^s, \tag{2}$$

where A is a constant related to the total surface area of the objects and s = -4 for point-focus SAXS sytems and s = -3 for line focus systems [28].

$I_N(q)$ is of primary interest and represents the intensity due to nanostructural features in the size range readily accessible by the slit geometry of the apparatus, from about 1 nm to about 30 nm for our slit settings. If the scattering object is a well-defined "particle" of volume v and uniform electron density n_p imbedded in a matrix of uniform electron density n_m, then $I_N(q)$ for a single particle can be expressed in terms of a form factor P(q) determined by the shape of the particle:

$$I_N(q) = Cv^2(n_p-n_m)^2\, P(q)^2\,, \qquad (3)$$

where C is a constant depending on choice of units. A wide variety of particle shapes and their associated form factors have been considered in the interpretation of small-angle data [28]. The total intensity from a distribution of particles of the same shape is obtained by superposition via Eq.3. If the particle density is high or the particles are correlated in position due to some type of interaction, then interparticle interference will influence $I_N(q)$ and a pair correlation structure factor S(q) can be included as a multiplicative factor [28]. Experimental evidence for this effect is a maximum or "shoulder" in I(q) not expected from P(q) alone.

Within the so-called "two-phase" model of particles+matrix a general "sum-rule" is valid for a randomly-oriented collection of particles with any shape, size distribution, and spatial correlation: for point focus geometry,

$$\int I_N(q)q^2dq = 2\pi^2\Omega(n_p-n_m)^2f(1-f) \equiv Q\,, \qquad (4a)$$

and for line-focus geometry satisfying the so-called "infinite-slit" condition [28],

$$Q = (q_s/2)\int I_N(q)qdq\,, \qquad (4b)$$

where Ω is the average atomic volume of the sample, f is the particle volume fraction, and q_s is a geometrical factor controlled by the slit conditions. The intensity $I_N(q)$ must be expressed in absolute electron units (electrons/atom) and the integration should extend from sufficiently low to sufficiently high limits of q so that negligible error occurs. Extrapolations based on the Guinier approximation [28] at low q and the power law (q^{-4} or q^{-3}) at high q can be used to make corrections or estimate possible errors.

We have found that most of the SAXS-detected features in the examined films can be modelled with either spherical- or ellipsoidal-shaped objects. The latter can mimic rod-like or plate-like objects through appropriate choice of major-to-minor axis ratio, while a preferred orientation will lead to readily observed [3,7,11,12,15,16,24-26] and modelled [3,28,29] anisotropies in the SAXS. In those cases where interparticle interference is evident in our data, usually in the a-SiC:H alloys, a hard-sphere pair correlation model for the structure factor (e.g., the Percus-Yevick solution [30]) can often account for the observed $I_N(q)$.

The third term contributing to the SAXS intensity (Eq.1) is that due to diffuse scattering, I_D. It has a variety of sources, all of which are at the atomic scale so that there

is little or no q dependence over the typical experimental range of q. Although I_D is weak, it is readily detectable in our experiments by either a nearly q-independent intensity over a wide range of q or the approach to a constant intensity level at high q. Possible sources for this intensity include thermal diffuse scattering [31], static disorder scattering [28], Compton incoherent scattering [32], and Laue monotonic scattering [33,34]. The latter is of interest due to its simple theoretical expression for a random alloy. For example, for a random binary alloy consisting of elements a and b, atomic numbers Z_a and Z_b, and atomic fractions C_a and C_b, the Laue monotonic intensity in electron units is

$$I_{lm} = C_a C_b (Z_a - Z_b)^2. \quad (5)$$

This contribution typically dominates I_D unless one is dealing with a single element sample. Significant deviations from this theoretical prediction may be attributed to alloy clustering (prediction is too low) or ordering (prediction is too high) via the use of short-range order parameters [34].

The ternary Si-Ge-H and Si-C-H alloys can be expected to have larger contributions to the SAXS from I_D due to the Laue monotonic scattering. For perfectly random $a_{1-x-y}b_xc_y$ alloys one finds, in analogy with Eq. 5,

$$I_{lm} = (Z_a-Z_b)^2(1-x-y)x + (Z_b-Z_c)^2xy + (Z_a-Z_c)^2(1-x-y)y. \quad (6)$$

Thus, measurement of systematic variations in the diffuse component with alloy composition may lead to information on deviations from alloy randomness.

4. EXPERIMENTAL METHODS

The SAXS apparatus used for our work is a line-focus Kratky-type small-angle system attached to a 12 kW rotating anode x-ray generator [17]. A graphite monochromator selects the Cu-Kα x-rays (λ=0.15418 nm) and the typical intensity incident on the sample is 1.5×10^8 photons/s in the form of a beam with 0.13 mm x 14 mm cross-section. Data are collected in a step-scannning mode over a range in 2θ from 0.13° to 8.8°, corresponding to q from 0.09 to 6 nm^{-1}. A low-noise detection system, coupled with long signal averaging and sometimes multiple scans, lead to detectable count rates as low as 0.1 photon/s.

Most of our work has been done with films of 1 to 10 μm thickness deposited on 10-μm-thick, high-purity Al foil. The film+substrate is then folded into 8 layers to make a SAXS sample. Some work has been done with films deposited on thin c-Si substrates

(~70 μm) to test whether significant differences in nanostructure occur for the two type of substrates. So far we have found only evidence of differences in surface roughness or a more preferred orientation of columnar-like structure on the flatter c-Si. The disadvantages to the thin c-Si substrates are the difficulty in handling, that only one layer can be used (due to absorption), and the problem of depositing high-quality layers thicker than about 2 μm without flaking from the substrate. The advantage is the very weak SAXS from c-Si itself. The Al foil has a significant small-q component due in part to double-Bragg scattering [35] that can reduce the accuracy of the small-q SAXS extracted from the film itself. This effect is relatively insensitive to heat treatment but we always use a piece of Al foil for a reference scan that was part of the same substrate during deposition and therefore experienced the same thermal history.

The raw SAXS intensity is converted into a normalized intensity as described elsewhere [17]. This can be converted into absolute electron units (eu or electrons/atom=e/a) on the basis of an average atomic or molecular volume, the linear absorption coefficient of the film, and the geometry of the SAXS beam and detector slit [36]. This conversion has been carefully checked by measuring the known SAXS of H_2O [37], which consists of only a q-independent diffuse intensity that is relatively strong. This experiment was done by mounting the water in a fused silica capillary tube after first making a SAXS scan from the empty capillary for reference. The SAXS data are shown in Fig. 1 for both the H_2O and the a-SiO_2 capillary tube. Both sets of data (presented in eu) are in good agreement with the prior data obtained at the Oak Ridge National Center for SAXS Research [37,38]. Note that the a-SiO_2 does not show any rise in the SAXS intensity at low q showing the absence of microvoids or other nanoscale density fluctuations in this type of amorphous material. The increase in SAXS as q increases is due to the approach to the first peak in the x-ray diffraction pattern of a-SiO_2 (short-range order effect corresponding to first peak in radial distribution function).

By conversion to absolute intensity units so that Eq.4 can be used directly without need of calibration (as we have done in the past using flotation densities [17, 39]), it is possible to state a well defined detection limit for voids. Based on our present intensity detection limit for typical samples of a-Si:H it is possible to detect void fractions as low as 0.01 vol.%. Our previous reported void fractions were sometimes overestimated, particularly for weakly scattering samples [39] because the diffuse component of the SAXS was not recognized and the flotation densities were affected to an unknown extent by H alloying. Even for cases where voids may not be the origin of the SAXS or there is a preferred orientation of the scattering objects (so that Eq.4 cannot be used to find f), the integrated intensity Q is regarded as a useful quantitative measure of the degree of

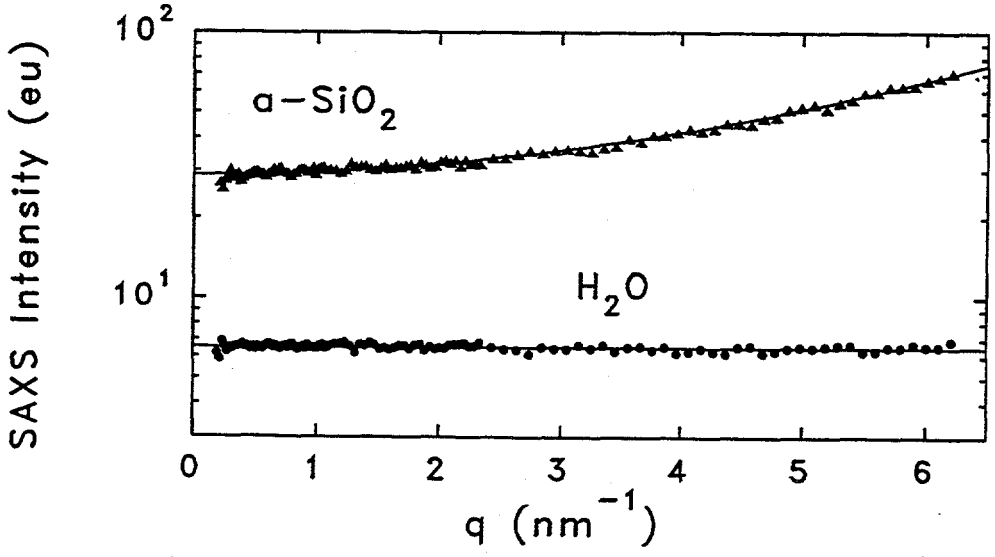

Fig. 1. SAXS data from water and fused silica capillary tube in electron units (electrons/H_2O molecule and electrons/SiO_2 molecule, resp.).

heterogeneity in the sample. We routinely check for oriented nanostructure by tilting the sample by an angle α relative to the x-ray beam and collecting another set of data $I_N(q, \alpha)$. Typically α=45° is used and the ratio r=Q(0°)/Q(45°) is a useful measure of the degree of preferred orientation. In addition, a new method developed during the last year consists of "rocking curve" measurements made by collecting intensity data versus α at a fixed q.

We routinely measure the mass density of the same films studied by SAXS using the flotation method [17], provided the density is below the upper limit allowed by available fluids. Measurements up to x=0.6 have been done with a-$Si_{1-x}Ge_x$:H alloys [15,16,26]. The observed density deficits compared to c-Si (2.329 g/cm^3), pure a-Si (2.287 g/cm^3) [40], c-$Si_{1-x}Ge_x$ alloys [41], diamond (3.52 g/cm^3), graphite (2.26 g/cm^3), or SiC (3.22 g/cm^3) can be helpful in interpretation of the SAXS and in determining the average effect of H alloying.

5. LOW-BANDGAP ALLOYS (a-SiGe:H)

A recent review discusses the universally observed problem of the degradation of opto-elecronic properties of a-$Si_{1-x}Ge_x$:H with increasing x [42]. As previously documented [16], Ge alloying above a fraction of about x=0.2 tends to induce a columnar-like nanostructure in a-$Si_{1-x}Ge_x$:H prepared by PECVD. This trend was demonstrated for films prepared by several groups [21]. In a recent study of films prepared at the Indian Association for the Cultivation of Science (IACS), the effect of H_2 dilution on this trend was investigated and it was found that, although the columnar-like features remained, they were definitely *reduced* by the dilution [26]. This is documented in Fig.2 where the integrated SAXS intensity Q (Eq.4) is shown as well as the tilt ratio versus the Ge fraction. Improved Urbach energies and photoconductivies correlated with these improved microstructures [26].

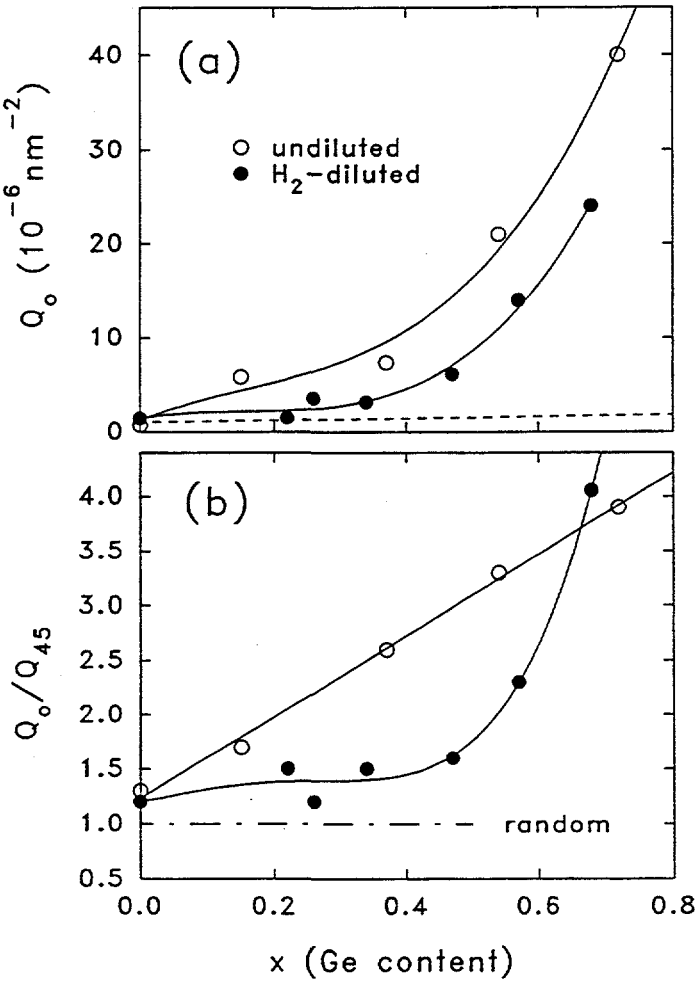

Fig. 2. (a) SAXS integrated intensities, Q_o, vs. Ge content and (b) the tilting effect ratio, Q_o/Q_{45}, vs Ge content. Lines drawn to guide the eye. [from ref. 26].

Here it is useful to contrast these results from IACS samples with those from two films prepared by USSC. These were prepared under different H_2 dilution conditions and the SAXS results are compared in Fig.3. The signals are much *stronger* from the high dilution sample and there is a *stronger* tilting effect. The "rocking curve" inset shows symmetry about zero tilt angle consistent with oriented features parallel to the film growth direction. The Q (Eq.4) is reduced by a factor 13 at a 45° tilt (vs 3.7 for the low dilution), much larger than is typically observed for any of the a-$Si_{1-x}Ge_x$:H films prepared earlier by USSC [23] or by other groups (factors of 2 to 5, see Fig.2) [21,26]. The results seemed so unusual that another deposition was made to test reproducibility. The duplicate sample behaved the same within experimental uncertainty. Particularly noteworthy is the fact that the conditions used to prepare the SAXS films are those used recently to prepare the i-layer of solar cells that show improved behavior for the high dilution condition compared to the low dilution condition [43]. Additional tests were made to search for possible microcrystallinity in the high dilution samples since the conditions are near those for inducing this type of growth [44]. Neither Raman spectroscopy, x-ray diffraction, or TEM revealed any evidence for microcrystallinity.

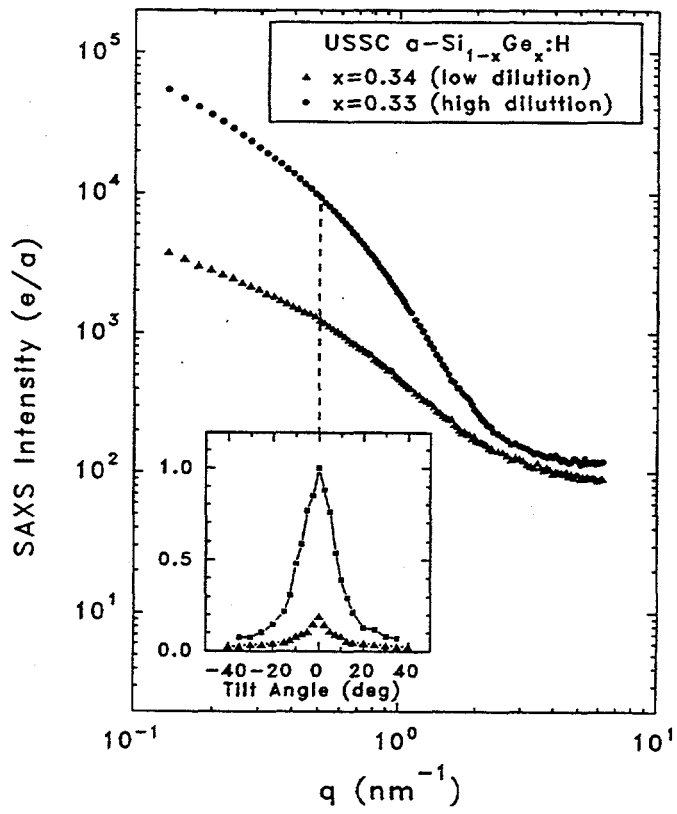

Fig. 3. SAXS data from two USSC alloys made with similar Ge contents, but different H_2 dilution. Inset shows effect of tilting on the SAXS intensity at q=0.5 nm^{-1} (dashed line).

The ellipsoidal model [28,29] was used to estimate shapes and volume fractions of the "phase" producing the strong SAXS. Assuming perfectly aligned voids with long axes parallel to the growth direction, the above tilt ratios yield major-to-minor axis ratios of 24 and 6 for the high and low dilution conditions, resp. The size distribution of the minor axis diameters is obtained from analysis of the non-tilted data and yields predominant diameters of 7 nm and 3 nm, resp. The above axis ratio therefore indicates objects as long as 0.17 μm in the high dilution sample.These features have not yet been detectable by TEM [45]. If we assume the ellipsoids to be voids, then the Q's, when analyzed within the oriented void model yields volume fractions of about 0.6% for *both* the high dilution and low dilution films. The flotation densities (3.28 and 3.31 g/cm^3 for the x=0.33 and 0.34 films) are both about 4% below crystalline density [41]. Thus H alloying, and a likely intrinsic density reduction for the amorphous state [40], are predominantly responsible for this density deficit.

If the objects are not voids but H-rich regions of non-zero electron density, then the volume fractions must be larger. We cannot rule out the possibility of Ge composition fluctuations as the source of the SAXS as suggested by other researchers [14] although our observed density deficits measured on the same films used for the SAXS [15,16,26] do show a trend of increasing deficit with x. Two Raman studies find evidence of non-random numbers of Si-Si, Si-Ge, and Ge-Ge bonds [46,47], while EXAFS results are contradictory [48,49]. An independent method to check for short-range clustering or ordering is to use the values of I_D found from a-$Si_{1-x-y}Ge_xH_y$ alloys for known x,y and compare with the prediction of Eq.6. Conversion of all the data into electron units from the films of several groups, as well as a set with y=0 (no H) prepared at CSM by magnetron sputtering leads to the results presented in Fig.4. The curves show predictions from Eq.6 for increasing amounts of H. All of the data agree quite well with these predictions and thus show *no evidence* for deviation from random atomic structure on the atomic scale. A method to search for longer-range Ge composition fluctuations would be the use of anomalous SAXS (ASAXS) at synchrotron facilities [50]. We are pursuing this approach through a collaboration with a group at the German synchrotron (DESY) and expect results in the next few months.

Through control of the ion bombardment during deposition, the group at Harvard has produced films on the Ge-rich side (x > 0.5) that show improved opto-electronic behavior [27]. Figure 5 shows SAXS data from two of these films as well as from an a-Ge:H film. Note the remarkable decrease in SAXS-detected nanostructure resulting from the low dilution conditions. The x=0.69 film shows no tilt effect while the x=0.75 and 1.0 films show a reduction in Q of only 1.5 at a 45° tilt. The void fraction of the x=0.69 film

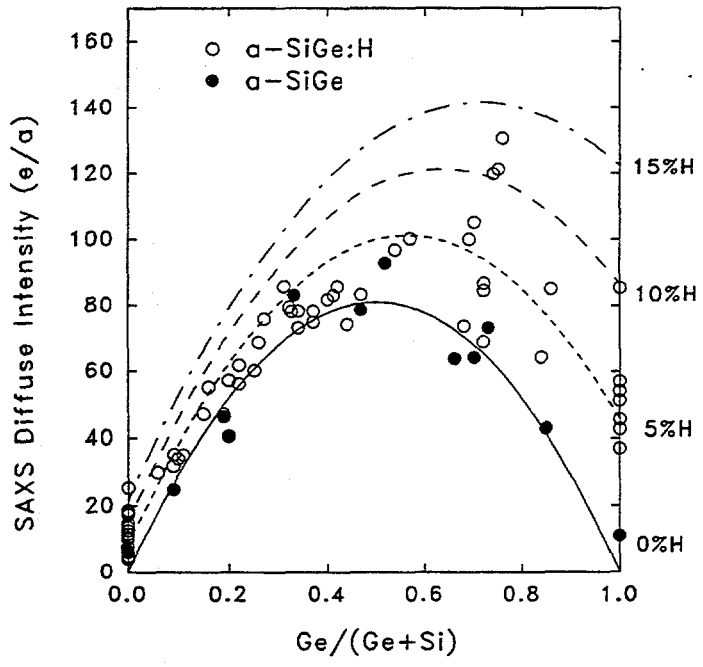

Fig. 4. Diffuse SAXS from a-$Si_{1-x}Ge_x$:H alloys and comparison with Laue monotonic theory for random alloys of various H content (solid and dashed curves).

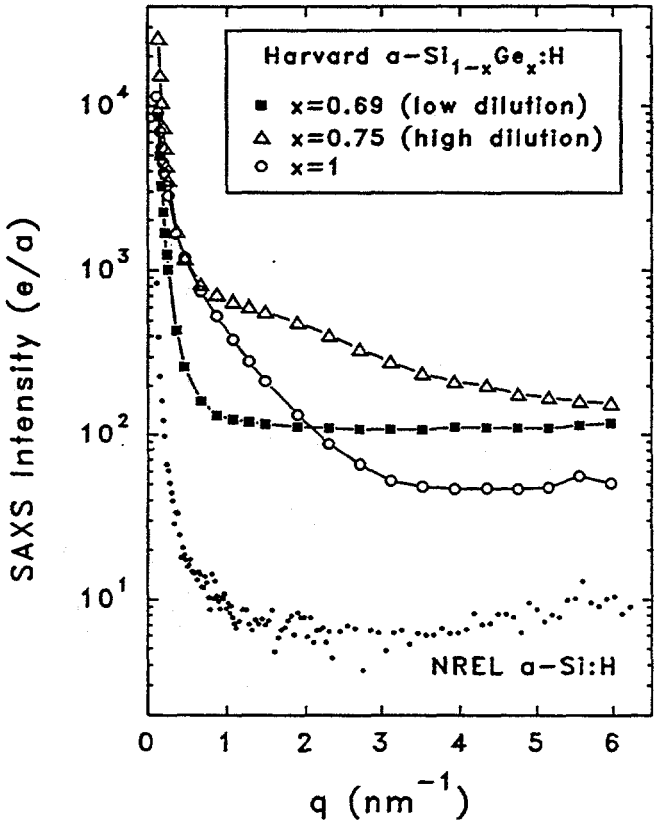

Fig. 5. SAXS from Ge-rich alloys prepared at Harvard University compared to data from device-quality a-Si:H (NREL sample, discussed below).

from Eq.4 is near our detection limit of 0.01% and therefore comparable to the lowest void fractions detected in a-Si:H. This result from high x films demonstrates that the previously observed trends of systematically increased heterogeneity with x on the Si-rich side of this alloy system [15,16,21,26 (Fig.2)] may be avoidable.

Films with x=1 (no Si) prepared by sputtering at Kaiserslautern University have extremely low SAXS-detected microstructure and large differences in surface roughness depending on the substrate used. Crystalline Si substrates yield smoother surfaces compared to the Al-foil substrates and microvoid fractions are well below 0.01 vol.%. These results correlate with low Urbach energies (<50 meV).

6. MID-BANDGAP MATERIALS (a-Si:H)

Figure 6 compares SAXS data expressed in electron units from a PECVD film made at the National Renewable Energy Laboratory (NREL) to those from a c-Si wafer. The NREL film was deposited under the same conditions used to make the i-layer of solar cells with 10% initial efficiency [51] and represents the typical weak SAXS seen from a-Si:H made by several device-making groups [United Solar Systems Corp. (USSC), Solarex Corp., Advanced Photovoltaic Sytems (APS)]. The very weak SAXS from the c-Si is well accounted for by two diffuse scattering contributions, thermal diffuse [31] and incoherent Compton scattering [32], their theoretical sum given by the solid line passing through the data. The data from the a-Si:H show an order-of-magnitude increase in the diffuse scattering and a clear rise in intensity with q below 1.5 nm^{-1}. For comparison, the expected SAXS from a 0.1 vol.% fraction of voids that are spheres of radius R=0.5 nm or 2.0 nm are shown. This makes clear that if such voids are present they are well below 0.1 vol.%. A fit to the data with Eq.1 shows that most of the signal is accounted for by $I_L(q)$ + I_D . Only a small contribution from $I_N(q)$ is needed and if it is assumed to be due to voids,

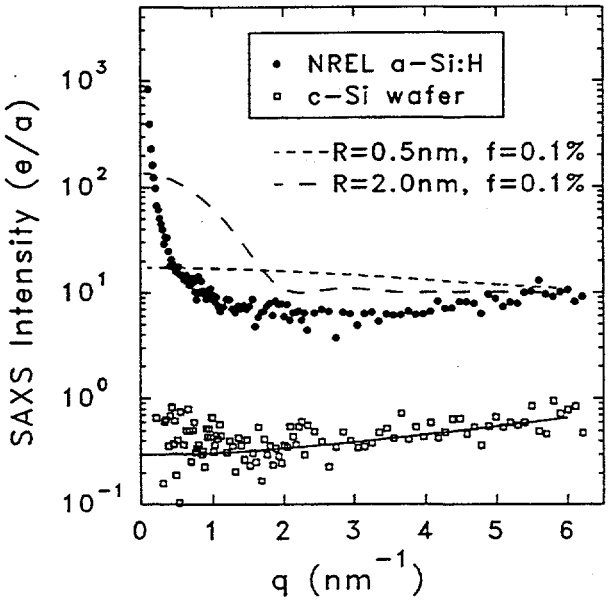

Fig. 6. SAXS data from PECVD a-Si:H (NREL #S940307-71i, no H_2 dilution, T_s=215°C, 4.5 μm thick)

then Eq.4 yields a volume fraction of less than 0.01%. The contribution from the large-scale structure, $I_L(q)$, is such that it can be accounted for by surface roughness of the magnitude observed by SEM [52] or STM [53,54]. Recent studies of a-Si:H [55] and a-Si [56] prepared by ion implantation of a polished c-Si wafer show no evidence for a steep rise at low q nor do they show any evidence for nanovoids in the as-implanted states. These results will be discussed further below.

The much stronger diffuse scattering compared to c-Si seen in Fig.6 is due to two contributions: static disorder of the a-Si matrix and compositional disorder on the atomic scale due to the H alloying (i.e., Laue monotonic scattering). The latter can be calculated from Eq. 5. The H concentration in films deposited under the same conditions as the SAXS sample is about 10 at.%, so Eq.5 yields I_{lm}=15 e/a, significantly higher than experiment (~7-10 e/a from Fig.1). We have recently measured the contribution from static disorder in pure a-Si to be near 3 e/a in the fully relaxed state [56]. Thus the I_{lm} contribution based on Eq.5 is too large by at least a factor of 2. Theory which accounts for atomic volume differences in a binary alloy shows that I_{lm} will be reduced by substitution of an element with a smaller atomic volume [57]. Due to the much smaller Si-H bond length relative to that of Si-Si, we expect a significantly smaller atomic volume for H and therefore a smaller I_{lm} than predicted by Eq.5. Analysis of flotation density data for samples of known H content and small void fractions provides a H/Si atomic volume ratio of about 0.4 [25].

It is interesting to note that the NMR-detected "clustered" and "isolated" phases, found generally in device-quality PECVD films with about 60:40 volume fractions [58], must somehow be associated with the diffuse SAXS signal unless the clustered phase has such large-scale clusters (>30 nm) that it is the origin of the $I_L(q)$ term. Although this seems unlikely, it cannot be ruled out since Eqs.3 and 4 show that a large volume fraction of a second phase can be present and only weakly detected by SAXS if $n_p \approx n_m$. Also, SANS studies of sputtered films demonstrated a relatively large-scale H microstructure which was modelled with the H clustered in narrow (~0.35 nm) boundary zones surrounding low-H regions [20].

Figure 7 compares data from several a-Si:H films made by USSC. To see more clearly the low q behavior, a log-log plot is shown. The solar cell properties utilizing i-layer films made under nominally identical conditions have been reported [59,22]. The i-layers grown at either the high deposition rate (1.4 nm/s) or at the lower substrate temperature (T_s = 175°C) with low H_2 dilution conditions yield lower initial efficiencies and more light-induced degradation of the efficiencies. The SAXS data from these two films are fitted with a predominant contribution from $I_N(q)$ (Eqs.1,3) that can be modelled

with spherical voids (the SAXS is isotropic) averaging near 1 nm in diameter. Application of Eq.4 yields void fractions of about 1 vol.% and 0.2 vol.% for the films made at a 1.4 nm/s deposition rate and at the T_s=175°C, low dilution conditions, resp. Since the q-dependence due to the small scattering objects persists up to the highest angles, the diffuse component from these two samples is difficult to pin down precisely, but it does appear larger than the other three samples in Fig.7 (which are near the value of the NREL sample in Fig.6).

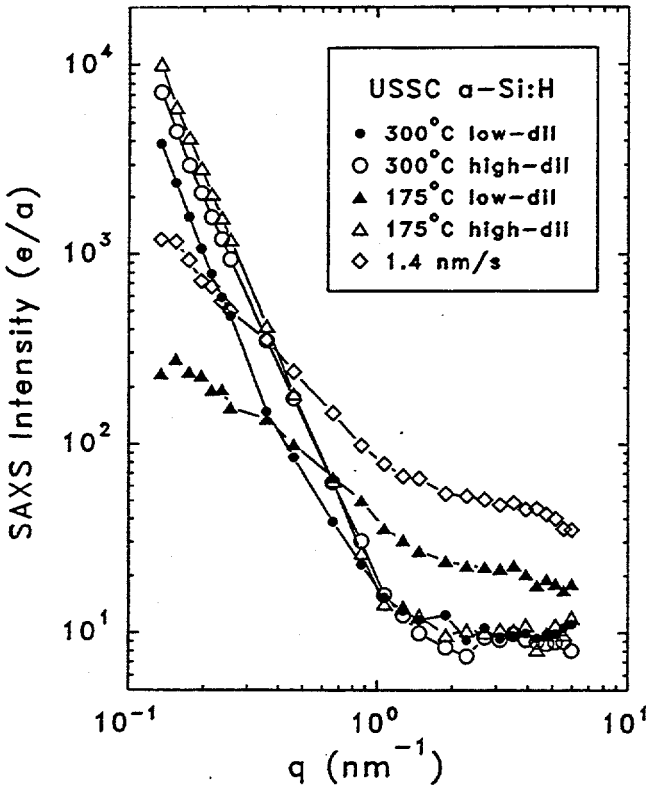

Fig. 7. Log-log plot of SAXS data from PECVD films made by USSC under various conditions as indicated.

The clear difference in SAXS caused by the use of the high H_2 dilution at T_s=175°C is worth noting. The intensity rises sharply at low q (with close to a q^{-3} Porod behavior-Eq.2), nearly identical to the behavior of the two films made at T_s=300°C. Because these three i-layer conditions yield similar, superior solar cell efficiency and stability [59], the steep rise at low q in these films deserves further examination. Comparison to the NREL sample in Fig.6 shows the signals to be about an order of magnitude stronger. The result of a tilt experiment with one of the samples (Fig.8) shows a sharp reduction in SAXS with tilting. This is characteristic of columnar-like features and similar results were found for the other two samples of Fig.7 with the steep low-q rise.

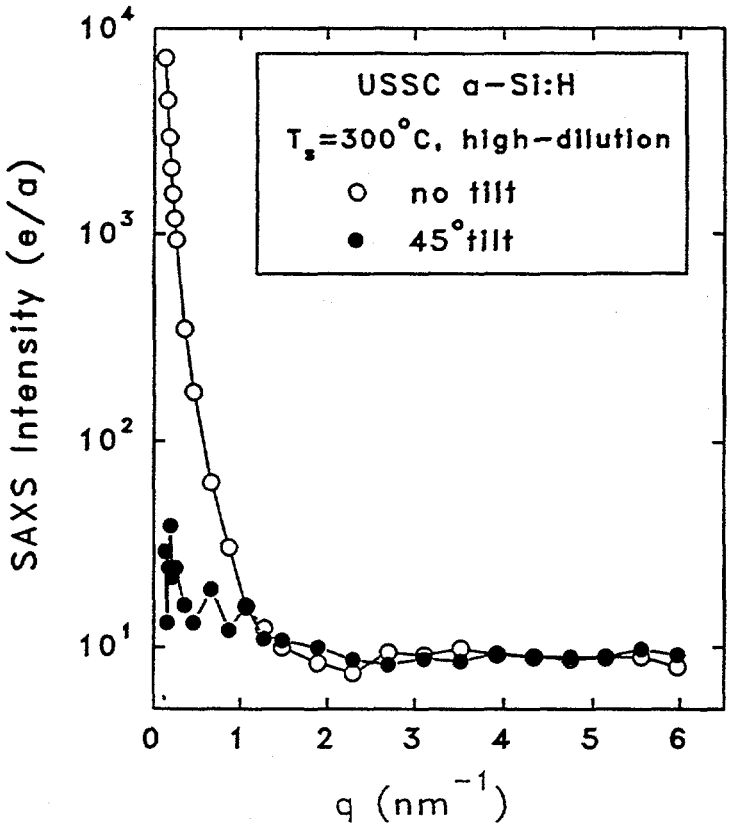

Fig. 8. Effect of tilt on SAXS from one of the USSC a-Si:H films.

Thus, it appears that device-quality i-layers with present state-of-the-art efficiencies and stabilties can have columnar-like behavior, as detected by SAXS. We emphasize that the observed signals are still much weaker than those from films made under conditions (e.g. low T_s) known to cause full-blown columnar microstructure as readily seen by electron microscopy [60]. The SAXS method is particularly sensitive to elongated features parallel to the growth direction since this leads to enhanced forward scattering (i.e. toward the detector). Figure 8 suggests that upon tilting the remaining SAXS is extremely weak, implying homogeneity of the film except for the residual columnar-like features. We found the tilting effect in device-quality a-Si:H to be variable depending on the source of the PECVD films. Table 1 compares the SAXS results for several device-quality PECVD a-Si:H films from different groups. Note the differences in the value of A (Eq.2) and the effect of tilting, while the values of Q and f (Eq.4) are all quite low and near our detection limit. The variability in A may be due to a predominance in either a surface roughness effect (no anisotropy in SAXS) or a residual columnar-like structure effect (anisotropy in SAXS) depending on deposition system and conditions.

Table 1. SAXS results from current state-of-the-art a-Si:H prepared by different groups

Group(Sample)	ρ(g/cm^3)	Q(eu/cm^3)	Q_o/Q_{45}	A (eu/nm^3)	I_D(eu)	<R>(nm)	f(%)
NREL(#S940307-71i)	2.245	8E21	1	0.8	7	~2	<0.01
NREL(#S940308-72i)	2.224	6E21	5	8	8	~2	<0.01
Solarex(#D1203-2)	2.222	<1E22	--	1.0	7	--	<0.01
Solarex(#D1203-3)	2.214	2E22	--	0.5	9	~2	0.01
APS(#B751)	2.238	4E21	>10	4.5	8	~2	<0.01
APS(#A323)	2.234	6E21	9	3.0	9	~2	<0.01
USSC(#6403)	2.244	<1E22	--	8	9	--	<0.01
USSC(#6407)	2.225	<1E22	>10	15	8	--	<0.01

We next describe some new data from hot-filament CVD a-Si:H ("hot-wire" a-Si:H). Our first report of SAXS from hot-wire films indicated larger void fractions compared to PECVD films [12]. However, those films were grown at substrate temperatures that yielded H contents similar to conventional PECVD films (8-12 at.%). Figure 9 shows data from one of those films compared to those from a more recent film typical of ones showing much lower H contents (2-3 at.%) and improved stability [61].

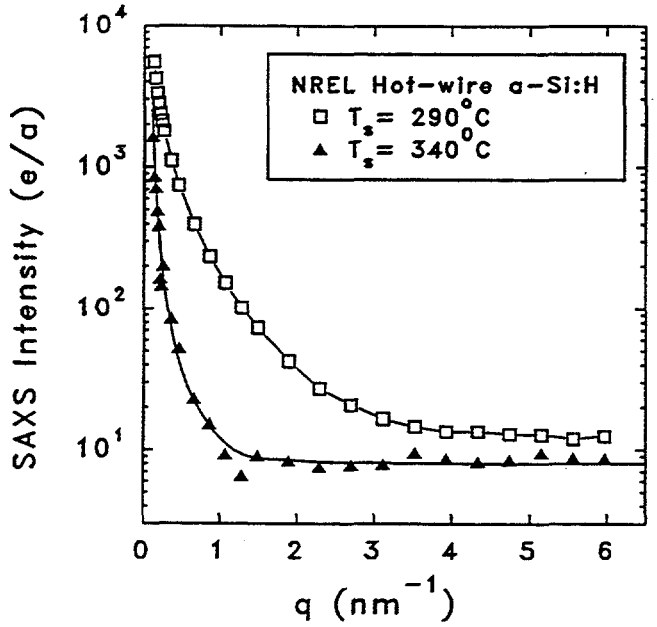

Fig. 9. SAXS data from NREL films made by hot-filament CVD at two substrate temperatures. The higher T_s film was deposited on a 70 μm c-Si wafer.

The flotation densities of the two films in Fig.9 are 2.18 g/cm^3 (T_s=290°C) and 2.29 g/cm^3 (T_s=340°C). The SAXS from the latter film is comparable to that from the PECVD film in Fig.6 and from those in Fig.7 with the lowest intensities. A fit to the T_s=290°C sample yields a void fraction of about 0.5 vol.% and an average diameter (assuming spheres) of about 4 nm. The maximum void fraction in the T_s=340°C film is 0.01 vol.%, assuming that the contribution of the q^{-3} term at low q is not due to voids. Device work is underway with hotwire material made under these conditions [51].

Films prepared by IACS under various amounts of Ar dilution (0% to 99%) is under study since improved photovoltaic behavior has been observed under 85-95% dilution conditions [62]. According to IR, TEM, PDS, and CPM, such films have less microstructure and fewer defects than films made without Ar dilution or at extreme Ar dilution (99%, where microcrystallinity appears depending on plasma power). Table 2 summarizes all the opto-electronic, composition, SAXS and flotation density data for a systematic series of 7 samples.

Several observations can be made from the data in Table 2:

1) Samples AS2 and AS12 have the poorest overall opto-electronic properties and they show the strongest SAXS Q's and largest void fractions f's. These two samples also have the smallest scattering centers as indicated by the volume-weighted average radii, <R>. TEM micrographs also show these two samples to be less homogeneous with AS12 having a clear columnar-like structure, consistent with the rather large SAXS tilt ratio.

2) The three samples (AS14, AS4, AS5) with the lowest defect densities, N_d, Urbach energies, E_o, and IR microstructure fractions, R, also have the lowest void fractions, comparable to the NREL sample. Note that there is not much variation in the photoconductivity, s_p, among all the samples.

3) The index of refraction, n, is largest for the sample with the weakest SAXS and lowest value of A (AS4). The flotation densities are surprisingly independent of the H concentration, C_H. Note in particular that the increase from 7.0 at% with no Ar dilution to ~20 at.% with Ar dilution does not produce a less dense film. The group at IACS attributes this to the effects of excited Ar-atom bombardment during growth of the films such that weak Si-Si bonds are broken and passified by the high H contents. They are also developing a two-phase model to account for the differences in the Urbach energy determined by PDS and CPM [62].

4) The diffuse SAXS intensity, I_D, is significantly larger than that from the NREL film and this is consistent with the much larger H content (except for AS1) according to Eq.5. However, the quantitative prediction from Eq.5 does not agree with the observed values and is thought to be related to the much smaller atomic volume of H compared to Si.

Further work on the explanation of the diffuse SAXS intensities of all the a-Si:H films is underway.

Table 2a. Opto-electronic data from IACS a-Si:H films made by PECVD under Ar dilution.

Sample	Ar (%)	C_H (at.%)	n	R(IR)	α(890cm^{-1}) (cm^{-1})	σ_d (S/cm)	σ_p	E_o(PDS) (meV)	E_o(CPM)	N_d(CPM) (10^{15}cm^{-3})
AS1	0	7.0	3.23	0.13	144	6.2E-11	3.8E-5	52	52	12
AS2	50	19.0	3.29	0.11	170	2.5E-11	6.1E-5	66	57	22
AS14	85	19.6	3.30	0.10	170	2.0E-10	5.0E-5	47.7	46.3	3.5
AS4	90	18.7	3.33	0.10	170	1.2E-10	4.8E-5	46.8	44.2	2.7
AS5	95	22.0	3.25	0.06	146	6.2E-11	8.3E-5	48.6	43.4	2.0
AS15	98	25.4	3.22	0.17	301	5.3E-10	6.0E-5	64.6	47.3	7.0
AS12	99	35.7	3.03	0.26	381	1.0E-9	6.9E-5	67.7	47.3	12

Table 2b. SAXS and flotation density results from IACS films. Data from one NREL film (sample shown in Fig.6 and Table 1) included for comparison.

Sample	Ar (%)	density(g/cm^3)	Q(eu/cm^3)	A (eu/nm^3)	I_D(eu)	<R>(nm)	f(%)
AS1	0	2.200 2.201[a]	4.4E22	0.7	17	1.9	0.03
AS2	50	2.194 2.203[a]	20E22	1.0	17	1.3	0.11
AS14	85	2.224 2.224[a]	2.2E22[b]	0.4	12.5	3.1	0.01
AS4	90	2.213	0.8E22	0.03	11.5	4.9	<0.01[c]
AS5	95	2.224	3.8E22	0.8	13	2.2	0.02
AS15	98	2.218	3.3E22	1.8	12.5	2.0	0.02
AS12	99	2.198	11E22[d]	7.5	12.5	1.7	0.06
NREL-71i	0	2.245	0.8E22	0.8	7	~2	<0.01[c]

a. repeat measurements; b. ratio Q(0)/Q(45)=1.1; c. lower limit of detection estimated to be 0.01%; d. ratio Q(0)/Q(45)=4.2

The role of ion bombardment during deposition is under study by the group at the University of Illinois using the technique of reactive magnetron sputtering which is their specialty. The flux of ions is varied using the "unbalanced magnetron" technique which uses weak magnetic fields to alter the plasma density above the substrate; the ion energy is varied using applied dc biases . The energy of the sputtered neutrals can be further altered by changing the Ar gas pressure. The goal is to correlate SAXS and spectroscopic ellipsometric data and provide clues to the mechanisms by which the growth surface starts to incorporate defects such as microvoids.

A set of SAXS samples was prepared to first examine the microstructure of the films without H present and the data are shown in Fig. 10. Clear differences are seen depending on the position of the substrate (middle vs left) and on the pressure (#1-high, #2-low). The middle position at low Ar pressure yields the most dense film as demonstrated by both the SAXS and flotation density data provided in Table 3. Note the lower diffuse intensities in these unhydrogenated a-Si films compared to those in Table 2. Note also that the #2-middle sample has a mass density less than 1 % below that of c-Si (2.33 g/cm^3). Comparison to the spectroscopic ellipsomtery data is underway.

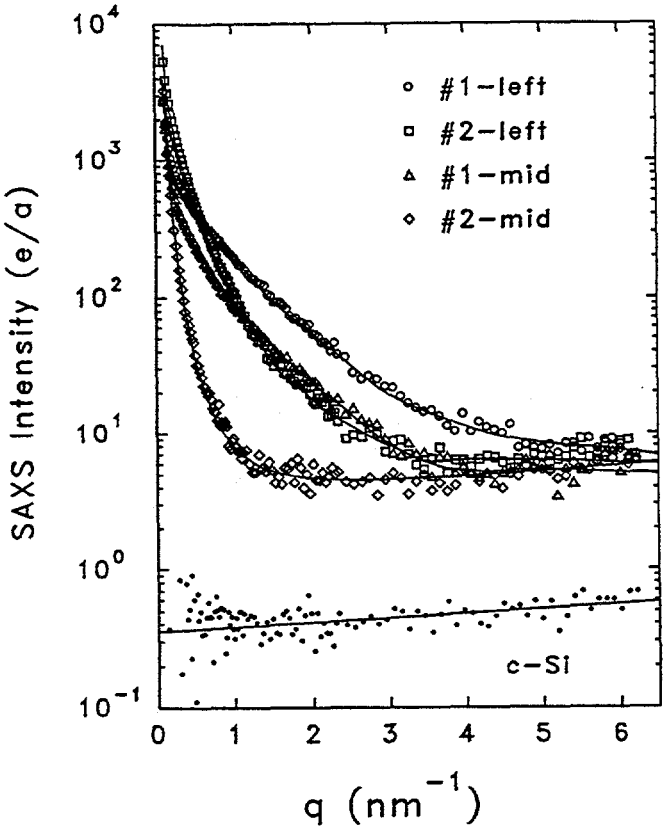

Fig. 10. SAXS data from Univ. Illinois a-Si films prepared under different ion bombardment conditions. Data from a c-Si wafer are shown for reference.

Table 3. SAXS and flotation data from Illinois a-Si samples. The void fraction f has been corrected using the tilt ratio.

Sample	density(g/cm^3)	Q(eu/cm^3)	Q_0/Q_{45}	A (eu/nm^3)	I_D(eu)	<R>(nm)	f(%)
#1-middle	2.288	4.1E23	3.4	3.4	5.0	1.8	0.09
#1-left	2.280	1.1E24	2.9	3.0	5.7	1.5	0.25
#2-middle	2.321	≤1 E22	1.9	4.0	4.0	--	<0.01
#2-left	2.274	6.3E23	1.3	5.0	6.0	3.7	0.28

Unusual deposition conditions are being explored at Ecole Polytechnique involving either helium dilution or hydrogen dilution at high depostion rates (1.5 nm/s) or low substrate temperatures (100°C). Some of these a-Si:H films have low defect densities ($\leq 1x10^{16}$ cm^{-3}) and low Urbach energies (≤50 meV). Table 4 shows results for two samples: EP101i (T_s=100°C, H_2 dilution, N_d(PDS)=6E15 cm^{-3}, E_o=50 meV, 0.4 nm/s) and EP212i (T_s=300°C, He dilution, N_d(PDS)=1E16 cm^{-3}, E_o=47 meV, 1.5 nm/s). Both samples have relatively high H contents of 18-19 at.% according to IR analysis. The SAXS signals are unusually low for such deposition conditions compared to prior results [11,22]. Note the significant differences in the A and I_D values implying differences in some large-scale structure and atomic-scale structure, respectively.

Table 4. SAXS and flotation density data for two Ecole Polytechnique a-Si:H films.

Sample	density(g/cm^3)	Q(eu/cm^3)	Q_0/Q_{45}	A (eu/nm^3)	I_D(eu)	<R>(nm)	f(%)
EP101i	2.19	<1E22	1.7	3.0	12.6	--	<0.01
EP212i	2.21	1.8E23	1.0	0.3	20	--	0.10

We now describe our recent studies of a-Si and a-Si:H prepared by ion implantation of c-Si [55,56]. Three samples have been prepared for systematic investigation by SAXS, SIMS, and IR as a function of annealing at temperatures up to 550°C. The first sample was pure a-Si prepared by implantation of Si ions with energies up to 17 MeV to generate a thick amorphous layer 8mm thick. The other two samples were hydrogenated by implantation of H ions to two distinct average concentrations, 1 at.% and 9 at.%. Figure 11 show the SAXS data from the a-Si sample together with theoretical curves. Data from the as-implanted a-Si are compared to those after 150 and 400°C anneals and with those

from a c-Si reference. The dashed lines represent the SAXS intensities expected from a random distribution of 0.1 vol.% nanovoids of radii 0.5 or 1.0 nm. The theoretical curves were obtained using the known form factor P(q) [Eq.3] for spheres and applying the slit-smearing correction appropriate for our line-focus geometry [36]. A constant baseline intensity was added to these curves to account for the observed diffuse scattering and to allow a clear comparison to the experimental data.

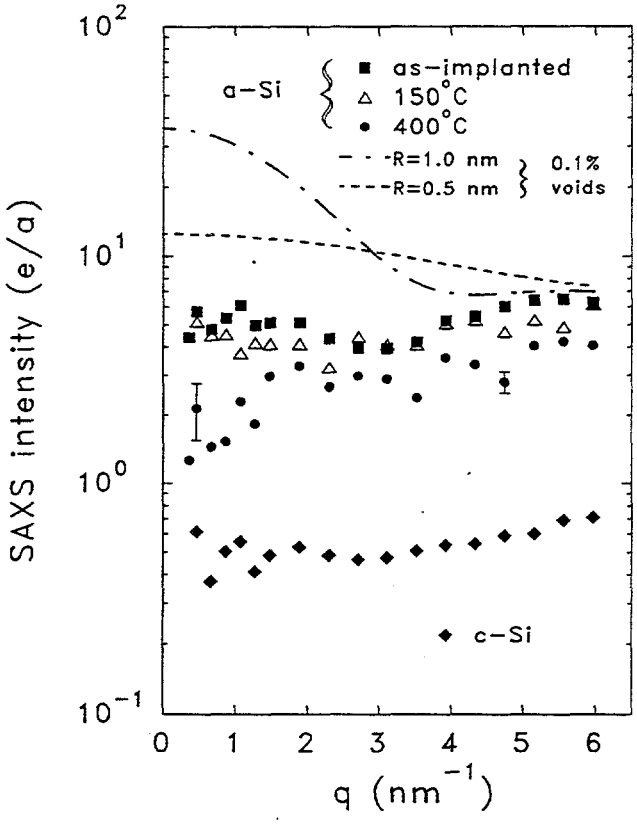

Fig. 11. SAXS intensities from a-Si prepared by ion implantation for the as-implanted state and after annealing for 1 h at 150 and 400°C.

Upon examination of Fig.11 a number of observations can be made: (i) all experimental data points in the lower q region fall well below the expected intensities for 0.1 % void fractions for the two sizes shown (larger sizes would produce even higher intensities, but at smaller q); (ii) all experimental data are nearly independent of q (implying diffuse scattering only), and if there is a slope it is positive, not negative as characteristic of void scattering shown by the dashed curves; (iii) the diffuse scattering is much stronger from the a-Si than from the c-Si, but is reduced somewhat by thermal annealing. For an explanation of this third observation, a detailed analysis of all

contributions to diffuse scattering of x-rays, including those from point defects, is required and this will be done in a forthcoming paper [63]. Here, we want to emphasize the first two observations: both show that the volume fraction of nanovoids is well below 0.1% and we therefore conclude that a-Si prepared by self implantation is homogeneous on a nm length scale. We also conclude that voids do not spontaneously appear in pure a-Si, even after prolonged annealing up to 540°C. Thus, nanometer-sized voids and increases in SAXS at low q are not intrinsic to the structure of pure a-Si and, therefore, structural features observed in deposited films of a-Si are most probably artefacts of the preparation methods.

To further illustrate this point, refer to Fig.10 where the SAXS from all of the Illinois sputtered a-Si films increases dramatically at low q in contrast with the a-Si data in Fig.11.

The result that no voids are present in this type of pure a-Si allows us to rule out this mechanism for the known density deficit of 1.8±0.1% [40]. The most likely remaining mechanism is an increase in the average Si-Si bond length of 0.6%[56]. The lack of voids also raises doubts about theoretical predictions of thermodynamically stable void structures in a-Si [64].

Results from the two hydrogenated samples with low (LH sample) and high (HH sample) average H contents are shown in Figs.12 and 13, respectively. First consider the LH sample whose SAXS data are compared with c-Si and the a-Si sample without H. Like the c-Si and a-Si samples there is essentially no q dependence in any of the LH data which implies that in the as-implanted and annealed states only diffuse SAXS occurs. SIMS data demonstrate that due to the non-uniformity of the implantation process, the local concentration of H in this sample reaches 3 to 4 at.% at certain depths (corresponding to the implantation energies used)[55]. Thus, we conclude that at least 3 to 4 at.% H is completely soluble in a-Si and the material is homogeneous on a nm scale.

In contrast, Fig.13 shows the SAXS from the as-implanted HH sample and the dramatic changes caused by the annealing. The as-implanted state displays only diffuse scattering, but much stronger than that from the LH sample. This is due to the Laue monotonic contribution (Eq.5) from the H alloying at higher concentrations. Annealing above 300°C induces systematic changes in the SAXS corresponding to the formation of low density nanostructural features of increasing size and volume fraction with temperature. The appearance of a maximum in the intensity is direct evidence of an interference effect due to a high density of scattering centers. The systematic drop in intensity at large q is attributed to the loss of H from the matrix which decreases the Laue diffuse scattering. To test for isotropy in the SAXS, the sample after the 500°C anneal

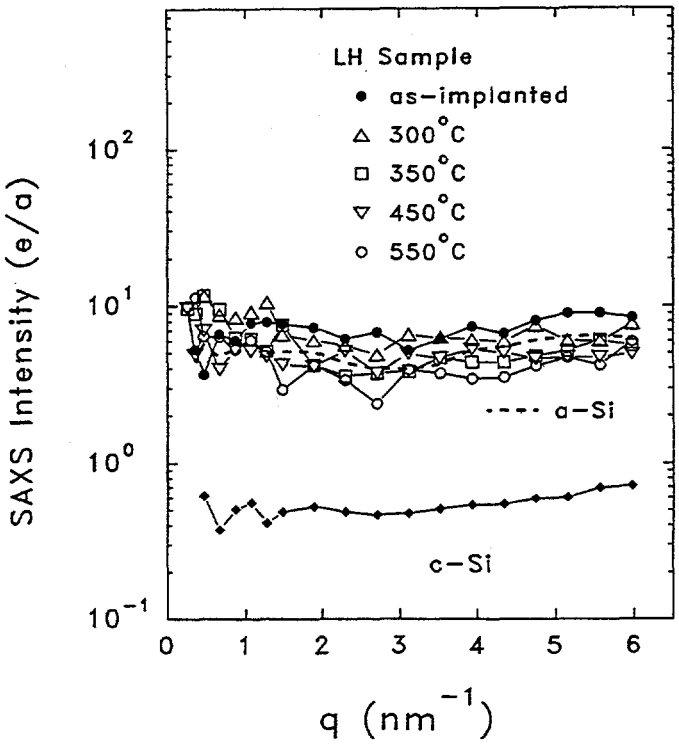

Fig.12. SAXS from a-Si:H(LH sample) prepared by ion implantation of Si and H ions compared to that from c-Si and a-Si (no H, same sample as in Fig.11).

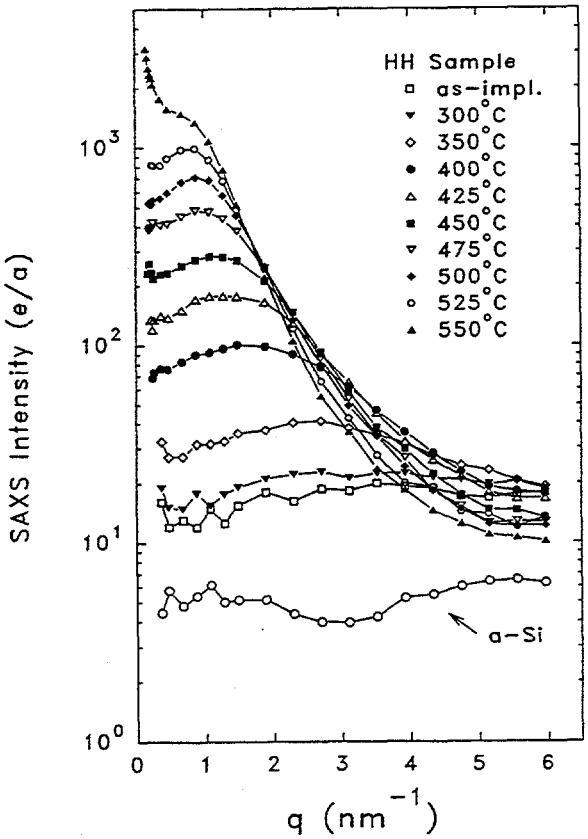

Fig.13. SAXS from a-Si:H (HH sample) prepared by ion implantation of Si and H ions. All anneals were for 4 h at the indicated temperatures.

was also measured in a tilted orientation (45^{o}). There was no change in the shape or intensity of the SAXS curve and this is consistent with either spherical scattering objects or randomly oriented non-spheres.

In order to obtain quantitative information on the size and volume fraction of the inhomogeneities as well as values of the diffuse component, the data for each anneal temperature were fitted with a theoretical intensity function corresponding to a distribution of spherical objects that are correlated in position by an effective hard-sphere interaction (Eq.3, including the pair-correlation function S(q))[28,30]. The fit parameters include the particle radii and an effective hard sphere diameter, D. The value of D is closely related to the location of the maximum in the SAXS intensity. To fit the data in Fig.13 it was necessary to include only 1 to 3 different sphere radii and the fits are essentially indistinguishable from the solid lines connecting the points in the figure. The total volume fraction of the heterogeneities, f, was determined from Eq.4 assuming two values of the electron density, zero (i.e., they are voids) and 9.7×10^{22} cm^{-3}. The latter value is that associated with a hydrogen pressure of 0.2 GPa in the heterogeneities, for which there is experimental evidence in the case of H_2 molecules in nanobubbles in a-Si:H [65]. The electron density of the matrix was taken as 5% lower than that of c-Si to account approximately for the H alloying and the intrinsic density deficit of 1.8% for a-Si [40]. Table 5 lists the results of the analyses of the SAXS data, including the average radius of the heterogeneities, <R>, D and the two f's based on the above assumptions. Both <R> and D increase linearly with anneal temperature and they both extrapolate back to zero at the same temperature of $264^{o}C$ suggesting this as the initial formation temperature of the inhomogeneities. A TEM investigation of the HH sample after the last anneal ($550^{o}C$) shows the presence of spherical-like objects with a diameter near 3 nm [45], in excellent agreement with the value of <2R> in Table 5.

A detailed analysis of the SIMS and IR data together with the SAXS results allows us to conclude that the H solubility is clearly exceeded in the HH sample where local concentrations reach 20 at.% and that the interpretation of the SAXS in terms of nanobubbles of precipitated H_2 molecules is the correct one [55]. It is concluded that H atoms can be accommodated in the a-Si matrix of *both* the LH and HH samples up to a concentration of only 3 to 4 at.% and this therefore represent the solubility limit of H in this type of a-Si. Recent results presented at the Spring'95 MRS meeting suggest a similar limit for a-Si:H prepared by PECVD [66]. Alloys with higher H contents are intrinsically unstable to two-phase separation upon annealing. Our recent SAXS study of the effect of annealing sputter-deposited a-Si:H containing about 10 at.%H also showed

increases in heterogeneity above 350°C [67] consistent with this solubility concept.

Table 5. Results of SAXS analyses of the annealed HH sample. T_A is the anneal temperature (all for 4 h), Q is the integrated intensity (Eq.4b), f_1 and f_2 are total volume fraction of nanobubbles based on zero and high-pressure H_2 electron densities, <R> is the volume-fraction-average radius of the nanobubbles , and D is the effective hard-sphere interaction diameter. I_D is the diffuse baseline intensity.

T_A (°C)	Q (10^{23}eu/cm^3)	f_1 (%)	f_2 (%)	<R> (nm)	D (nm)	I_D (e/a)
350	5.2	0.29	0.40	0.50	1.9	17
400	11.5	0.65	0.89	0.72	2.5	17
425	16.1	0.91	1.26	0.81	3.2	16
450	21.0	1.20	1.65	0.96	3.5	13
475	27.2	1.55	2.14	1.08	4.1	12
500	31.9	1.83	2.53	1.25	4.6	11.5
525	36.1	2.08	2.87	1.39	5.3	11
550	42.9	2.47	3.47	1.55	5.7	9.5

7. HIGH-BANDGAP ALLOYS (a-SiC:H)

As with Ge alloying, C additions lead to increased heterogeneity [17,18,68]. Since our first SAXS study from a series of PECVD a-$Si_{1-x}C_x$:H alloys was reported six years ago [17], we have continued to observe a high density of nm-sized scattering centers from this type of alloy. However, the use of H_2 dilution or deposition by reactive magnetron sputtering seems to help in significantly reducing their numbers [21]. Figure 14 illustrates the dramatic change in the SAXS caused by a relatively small amount of C (x=0.07) up to larger amounts (x=0.27). Since all intensities are reported here in electron units the results can be compared directly to those of a-Si:H and a-SiGe:H in the other figures. For the two films made by Solarex with and without H_2 dilution, there is a clear reduction in the amount of the smaller features (seen at higher q) even though x is larger with dilution. This improvement in the nanostructure correlates with a factor of 40 improvement in the $\mu\tau$ product. The highest x film was made by the group at Utrecht University. None of the samples show any anisotropy so the scattering centers are either spherical or randomly oriented non-spheres. The flotation densities of these films, 2.11 1.92, 2.05, and 1.72

g/cm^3 for x=0.07, 0.18, 0.23 and 0.27, resp., are indicative of either large amounts of H incorporation, large void fractions, non-diamond-like structure, or a combination thereof. Assuming voids, Eq.4 yields f=0.010, 0.034, 0.015, and 0.056, resp. Thus voids alone clearly cannot explain the low densities.

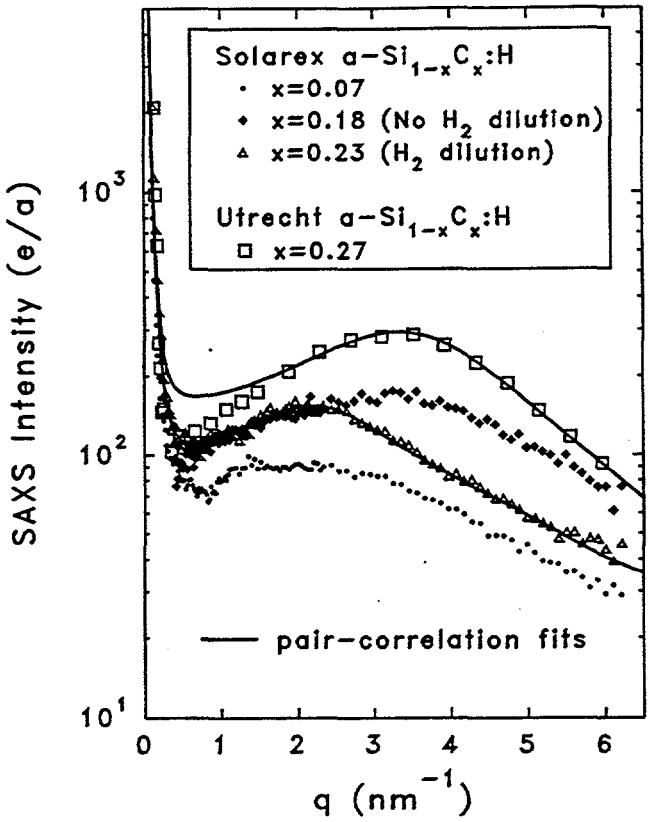

Fig. 14. SAXS from a-SiC:H alloys and fits to two (solid lines) including pair-correlation.

The scattering at high q and the presence of a broad maximum tell us that the objects are extremely small and the x-ray scattering shows an interference effect. The latter can be caused by either a sufficiently high density so that the objects are necessarily correlated in position via a "hard-sphere"-like interaction or by a lower density of objects that are correlated in position via some other, longer-range interaction. A fit of the hard-sphere pair-correlation model [30] of the structure factor, S(q), combined with a single-size sphere form factor, P(q) [Eq.3], yields the solid line fits shown in Fig.7 for the x=0.23 and 0.27 samples. The fits yield hard-sphere diameters of 2.3 and 1.5 nm [from S(q)], resp., which are larger than the diameters from P(q), both about 1 nm, suggesting an interaction between the particles. A possible interaction mechanism could be strain fields around the objects.

A set of a-SiC:H alloys doped with B via the RMS technique at the University of Illinois yields the SAXS results shown in Figs. 15a and b. The log-log plot shows more clearly the differences in low q behavior. Data from the NREL sample used for Fig.6 are included for comparison. One can see large differences in the diffuse SAXS compared to the NREL a-Si:H. This can be attributed to the higher degree of alloying and the high concentrations of H as determined by thermal evolution at Illinois (~20-40 at.%). The primary variable during deposition was the partial pressure of hydrogen and this is listed for each sample. Two samples were made at different substrate temperatures. Compositions of the films are listed in Table 6. There appears to be a problem with oxygen contamination as the hydgrgen partial pressure increases. The SAXS quantitative data as listed in Table 7 suggest a systematic increase in the void fraction with increasing hydrogen pressure. The three alloys made at the highest hydrogen pressure have the largest dark conductivity (1.5-6.7x10^{-6} /Ωcm) and larger optical gaps, but these are only 1.81-1.84 eV (Tauc), in spite of the C and H alloying. It is interesting to note that sample B3103 has the highest density we have observed yet for a-SiC:H and its void fraction is the lowest. However, its optical gap is only 1.43 eV. Due to the complex nature of these alloys the choice of the electron density of the matrix for use in the f calculations (Eq.4a) is not obvious. For the results in Table 7, the Si and C contents of Table 6 were used together with an assumption that the electron density associated with the C is an average of that for diamond and graphite. The values of f are typical for a-SiC:H alloys but the tilt ratios of greater than unity differ from PECVD films which always yield unity within experimental error (~± 0.2).

Table 6. Compositions of Illinois a-SiC:H(B) alloys from EPMA (at.%)

Sample(P_{H2},T_s)	Si	C	B	O
B3103(0.0,230)	66.2	32.4	0.3	1.1
B3102(0.6,230)	70.0	28.3	0.4	1.3
B3105(1.5,230)	79.4	15.8	0.3	4.5
B3106(4.0,230)	74.7	21.0	0.7	3.6
B3108(6.0,230)	81.5	8.5	0.1	9.9
B3107(8.0,230)	85.3	6.4	0.2	8.1
B3110(3.0,300)	61.3	26.7	5.9	6.1
B3111(0.6,150)	84.4	10.8	0.4	4.4

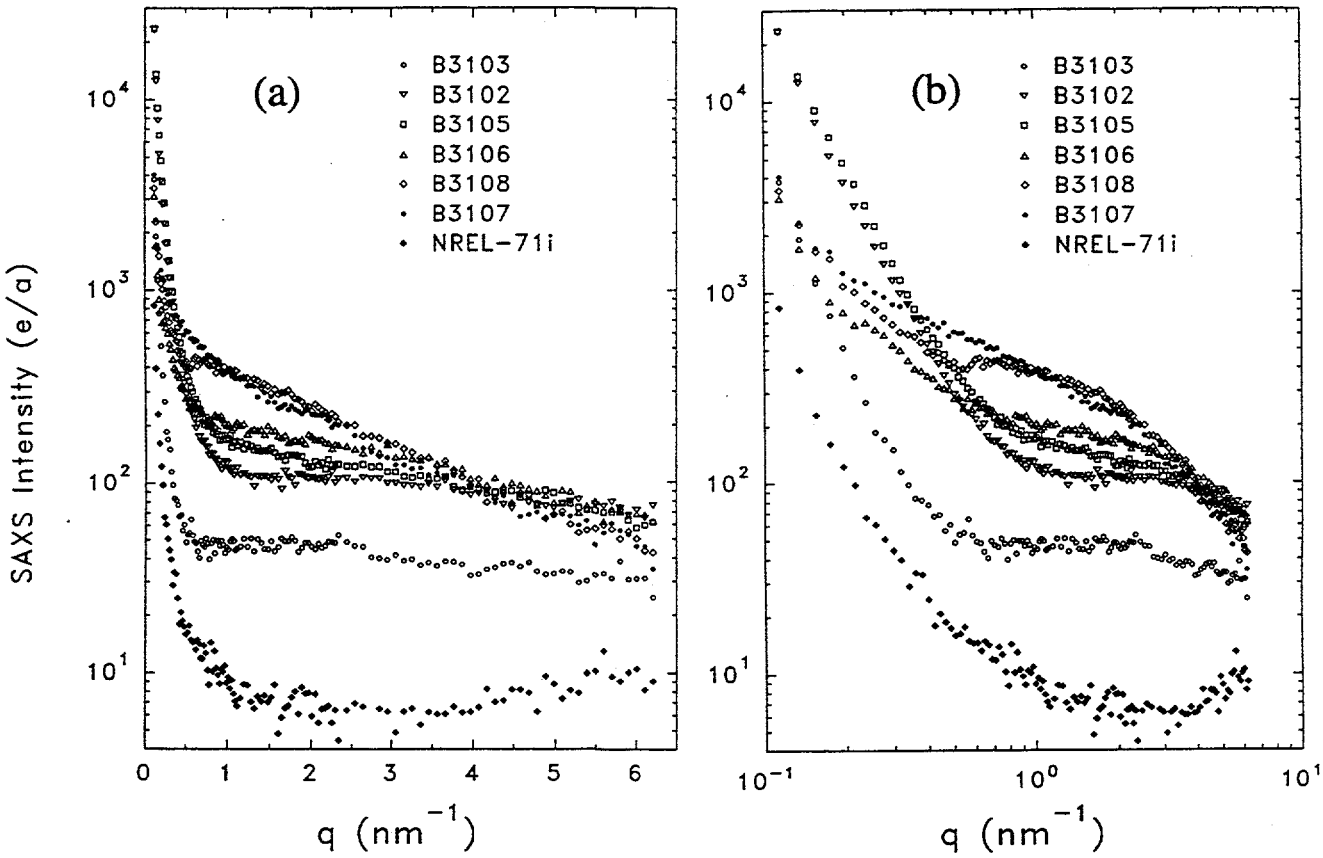

Fig. 15. SAXS from B-doped a-SiC:H alloys prepared by reactive magnetron sputtering at University of Illinois. (a) log-linear plot; (b) log-log plot.

Table 7. SAXS and density results for Illinois a-SiC:H(B) alloys

Sample	ρ(g/cc)	Q (10^{23}eu/cc)	Q(0)/Q(45)	f (%)
B3103	2.34	5.1	2.3	0.3
B3102	2.17	30	1.3	1.7
B3105	2.04	33	1.0	2.3
B3106	2.00	36	---	3.1
B3108	2.03	41	1.7	3.6
B3107	2.08	39	---	2.9
B3110	2.13	12	---	0.8
B3111	2.07	36	---	2.5

8. CLOSING REMARKS

Nanovoids or H-rich clusters with 1 to 4 nm sizes in a-Si:H that show little or no anisotropic SAXS correlate with poor solar cell and opto-electronic behavior. Larger-scale structures due either to surface roughness or residual columnar-like features are found in present state-of-the-art device material. Ge alloying above x=0.2 typically leads to an oriented nanostructure indicative of columnar-like growth while C alloying typically induces a random nanostructure consisting of a narrow size distribution of 1-nm-sized objects that may be correlated in position via some interaction. Recent device-quality a-$Si_{0.7}Ge_{0.3}$:H prepared by PECVD under high hydrogen dilution has shown an extremely-oriented structure that can be modelled with ellipsoidal objects that have major-to-minor axis ratios in excess of 20. These oriented objects and those in the a-Si:H are parallel to the solar cell tranport direction so it may be reasonable that such features may not be detrimental if they are sufficiently sparse, as indeed indicated by the SAXS analyses. Conditions of enhanced ion-bombardment during PECVD growth of high-Ge-content alloys ($x > 0.5$) recently led to films with no oriented nanostructure and SAXS signals that are comparable to those from the best a-Si:H.

Information on static disorder and atomic-scale composition fluctuations in these materials is being extracted from the diffuse component of the SAXS. Results from the a-$Si_{1-x}Ge_x$:H alloy system do not reveal any evidence of Si-Ge short-range clustering. Similar studies of a-Si:H with a wide range of H content and of a-SiC:H alloys are underway. Effects of thermal annealing on the SAXS-detected nanostructure in a-Si:H have recently been reported [67] and more efforts in this direction are providing information on the thermal stability of the nanostructure during hydrogen diffusion and evolution [55,56].

Acknowledgements

We thank all the groups who supplied the samples and relevant opto-electronic data for this research. CSM graduate students D. Min and T. Berens contributed to this work. Raman measurements by T.E. Furtak at CSM, TEM measurements by K.M. Jones at NREL, and composition measurements by A. Mason of NREL are gratefully acknowledged.

9. REFERENCES

1. S.C. Moss and J.F. Graczyk, Phys. Rev. Lett. **23**, 1167 (1969).
2. N.J. Shevchik and W. Paul, J. Non-Cryst. Solids **16**, 55 (1974).
3. G.S. Cargill, Phys. Rev. Lett. **28**, 1372 (1972).
4. N.J. Shevchik and W. Paul, J. Non-Cryst. Solids **8-10**, 381 (1972).
5. P. D'Antonio and J.H. Konnert, Phys. Rev. Lett. **43**, 1161 (1979).
6. T.A. Postol, C.M. Falco, R.T. Kampwirth, I.K. Schuller, and W.B. Yelon, Phys. Rev. Lett **45**, 648 (1980).
7. A.J. Leadbetter, A.A.M. Rashid, R.M. Richardson, A.F. Wright, and J.C. Knights, Solid State Commun. **33**, 973 (1980).
8. R. Bellissent, A. Chenevas-Paule, and M. Roth, J. Non-Cryst. Solids **59&60**, 229 (1983).
9. R. Vanderhaghen, B. Chaurand, and B. Drevillon, Thin Solid Films **124**, 293 (1985).
10. A.J. Craven, A.M. Patterson, A.R. Long, and J.I.B. Wilson, J. Non-Cryst. Solids **77&78** 217 (1985).
11. A.H. Mahan, D.L. Williamson, B.P. Nelson, and R.S. Crandall, Solar Cells **27**, 465 (1989).
12. A.H. Mahan, Y. Chen, D.L. Williamson, and G.D. Mooney, J. Non-Cryst. Solids **137&138**, 65 (1991).
13. S. Muramatsu, S. Matsubara, T. Watanabe, T. Shimada, T. Kamiyama, K. Suzuki, and A. Matsuda, Jpn. J. Appl. Phys. **30**, L2006 (1991).
14. S. Muramatsu, T. Shimada, H. Kajiyama, K. Azuma, T. Watanabe, T. Kamiyama, K. Suzuki, Jpn. J. Appl. Phys. **28**, L1092 (1989).
15. S.J. Jones, Y. Chen, D.L. Williamson, and G.D. Mooney, Mat. Res. Soc. Symp. Proc. **258**, 229 (1992).
16. S.J. Jones, Y. Chen, D.L. Williamson, R. Zedlitz, and G. Bauer, Appl. Phys. Lett. 62, 3267 (1993).
17. D.L. Williamson, A.H. Mahan, B.P. Nelson, and R.S. Crandall, Appl. Phys. Lett. **55**, 783 (1989).
18. M.N.P. Carreno, I. Pereyra, M.C.A. Fantini, H. Takahashi, and R. Landers, J. Appl. Phys. **75**, 538 (1994).
19. A. Chenavas-Paule, R. Bellissent, M. Roth, and J.I. Pankove, J. Non-Cryst. Solids **77&78**, 373 (1985).
20. R. Bellissent, in *Amorphous Silicon and Related Materials*, edited by H. Fritzsche (World Scientific, Singapore, 1988) p.93.
21. D.L. Williamson, Y. Chen, and S.J. Jones, in *12th NREL Photovoltaic Program Review*, AIP Conf. Proc. No. 306, Edited by R. Noufi and H.S Ullal (AIP, New York, 1994) p.442.
22. S. Guha, J. Yang, S.J. Jones, Y. Chen, and D.L. Williamson, Appl. Phys. Lett. **61**, 1444

(1992).

23. S.J. Jones, Y. Chen, D.L. Williamson, X. Xu, J. Yang, and S. Guha, Mat. Res. Soc. Symp. Proc. **297**, 815 (1993).
24. S.J. Jones, Y. Chen, D.L. Williamson, U. Kroll, and P. Roca i Cabarrocas, J. Non-Cryst. Solids **164-166**, 131 (1994).
25. S. Chattopadhyay, S.N. Sharma, R. Banerjee, D.M. Bhusari, S.T. Kshirsagar, Y. Chen, and D.L. Williamson, J. Appl. Phys. **76**, 5208 (1994).
26. A.R. Middya, S. Ray, S.J. Jones, and D.L. Williamson (submitted for publication).
27. P. Wickboldt, D. Pang, W. Paul, J.H. Chen, F. Zhong, J.D. Cohen, Y. Chen, and D.L. Williamson (submitted to ICAS'95).
28. see e.g., L.A. Fegin and D.I. Svergun, *Structure Analysis by Small-Angle X-ray and Neutron Scattering* (Plenum, New York, 1987), and references therein.
29. M. Shibayama, S. Nomura, T. Hashimoto, and E.L. Thomas, J. Appl. Phys. **66**, 4188 (1989).
30. N.W. Ashcroft and J. Lekner, Phys. Rev. **145**, 83 (1966).
31. B.E. Warren, *X-ray Diffraction* (Dover, New York, 1969) p.174.
32. A.J. Freeman, Acta Cryst. **12**, 929 (1959).
33. A.M. Levelut and A. Guinier, in *Small-Angle X-ray Scattering*, Edited by H. Brumberger (Gordon and Breach, New York, 1967) p.351.
34. L.H. Schwartz and J.B. Cohen, *Diffraction from Materials* (Springer, Berlin, 1987) p.402.
35. B.E. Warren, Acta Cryst. **12**, 837 (1959).
36. V. Gerold, in *Small-Angle X-ray Scattering*, Edited by H. Brumberger (Gordon and Breach, New York, 1967) p. 277.
37. R.W. Hendricks, P.G. Mardon, and L.B. Shaffer, J. Chem. Phys. **61**, 319 (1974).
38. J.B. Bates, R.W. Hendricks, and L.B. Shaffer, J. Chem. Phys. **61**, 4163 (1974).
39. A.H. Mahan, D.L. Williamson, B.P. Nelson, and R.S. Crandall, Phys. Rev. B **40**, 12024 (1989).
40. J.S. Custer, M.O. Thompson, D.C. Jacobson, J.M. Poate, S. Roorda, W.C. Sinke, and F. Spaepen, Appl. Phys. Lett. **64**, 437 (1994).
41. J.P. Dismukes, L. Ekstrom, and R.J. Paff, J. Phys. Chem. **68**, 3021 (1964).
42. W. Paul, J.H. Chen, E.Z. Liu, A.E. Wetzel and P. Wickboldt, J. Non-Cryst. Solids **164-166**,1(1993).
43. S. Guha and J. Yang (private communication).
44. S. Guha, J. Yang, P. Nath, and M. Hack, Appl. Phys. Lett. **49**, 218 (1986).
45. K.M. Jones, NREL (private communication).
46. M.B. Schubert and G.H. Bauer, Phil. Mag. B **62**, 59 (1990).
47. L. Yang, J. Newton, and B. Fieselmann, Mat. Res. Soc. Symp. Proc. **149**, 497 (1989).

48. L. Incoccia, S. Mobilio, M.G. Proietti, P. Fiorini, C. Giovanella, and F. Evangelisti, Phys.Rev. B **31**, 1028 (1985).
49. Y. Nishino, S. Muramatsu, Y. Takano, and H. Kajiyama, Phys. Rev. B **38**, 1942 (1988).
50. J.E. Epperson and P. Thiyagarajan, J. Appl. Cryst. **21**, 652, (1988).
51. R.S. Crandall, Yueqin Xu, A.H. Mahan, et al (private communication).
52. R.C. Ross, A.G. Johncock, and A.R. Chan, J. Non-Cryst. Solids **66**, 81 (1984).
53. A.W. McKinnon, S. Baker, and M.E. Welland, J. Non-Cryst. Solids **139**, 157 (1992).
54. D. Tanenbaum, A. Laracuente, and A.C. Gallagher, Mat. Res. Soc. Symp. Proc. **336**, 49 (1994).
55. S. Acco, D.L. Williamson, P.A. Stolk, et al (in preparation).
56. D.L. Williamson, S. Roorda, M. Chicoine, R. Tabti, P.A. Stolk, S. Acco, and F.W. Saris, Appl. Phys. Lett. (in press).
57. J. Peisl, H. Franz, A. Schmalzbauer, and G. Wallner, Mat. Res. Soc. Symp. Proc. **209**, 271 (1991).
58. J.B. Boyce and S.E. Ready, Physica B **170**, 305 (1991).
59. J. Yang, X. Xu, and S. Guha, Mat. Res. Soc. Symp. Proc. **336**, 687 (1994).
60. J.C. Knights and R.A. Lujan, Appl. Phys. Lett. **35**, 244 (1979).
61. A.H. Mahan and M. Vanecek, in *Amorphous Silicon Materials and Solar Cells*, AIP Conf. Proc. No.234, Edited by B.L. Stafford (AIP, New York, 1991) p.195.
62. P. Chaudhuri, private communication.
63. D.L. Williamson, S. Roorda, et.al. (in preparation).
64. R. Biswas, I. Kwon, A.M. Bouchard, C.M. Soukoulis, and G.S. Grest, Phys. Rev. B **39** (1989) 5101.
65. Y.C. Chabal and C.K.N. Patel, Rev. Mod. Phys. **59** (1987) 835.
66. J. Daey-Ouwens and R.E.I. Schropp, Mater. Res. Soc. Symp. Proc. (1995, in press).
67. J. Shinar, H. Jia, R. Shinar, Y. Chen, and D.L. Williamson, Phys. Rev. B **50**, 7358 (1994).
68. H. Efstathiadis, Z. Yin, and F.W. Smith, Phys. Rev. B **46**, 13119 (1992).

REPORT DOCUMENTATION PAGE

Form Approved
OMB NO. 0704-0188

1. AGENCY USE ONLY (Leave blank)	2. REPORT DATE	3. REPORT TYPE AND DATES COVERED
	August 1995	Annual Subcontract Report

4. TITLE AND SUBTITLE

Microstructure of Amorphous-Silicon-Based Solar Cell Materials by Small-Angle X-Ray Scattering

5. FUNDING NUMBERS

C: XAN-4-13318-04

TA: PV531101

6. AUTHOR(S)

D. L. Williamson

7. PERFORMING ORGANIZATION NAME(S) AND ADDRESS(ES)

Colorado School of Mines
Department of Physics
Golden, CO 80401

8. PERFORMING ORGANIZATION REPORT NUMBER

9. SPONSORING/MONITORING AGENCY NAME(S) AND ADDRESS(ES)

National Renewable Energy Laboratory
1617 Cole Blvd.
Golden, CO 80401-3393

10. SPONSORING/MONITORING AGENCY REPORT NUMBER

TP-411-8122

DE95009273

11. SUPPLEMENTARY NOTES

NREL Technical Monitor: W. Luft

12a. DISTRIBUTION/AVAILABILITY STATEMENT

12b. DISTRIBUTION CODE

UC-1262

13. ABSTRACT *(Maximum 200 words)*

This report describes work performed to provide details of the microstructure in high-quality hydrogenated amorphous silicon and related alloys for the size scale from the atomic up to about 30 nm. The materials studied were prepared by current state-of-the-art deposition methods as well as by new and emerging deposition techniques. The purpose is to establish the role of microstructural features in controlling the opto-electronic and photovoltaic properties. The approach centers around the use of the uncommon technique of small-angle X-ray scattering (SAXS), which is highly sensitive to microvoids and colunmar-like microstructure. Nanovoids or H-rich clusters with 1- to 4-nm sizes in a-Si:H that show little or no anisotropic SAXS correlate with poor solar cell and opto-electronic behavior. Larger-scale structures due either to surface roughness or residual columnar-like features are found in present state-of-the-art device material. Ge alloying above 20 at.% typically leads to an oriented nanostructure indicative of columnar-like growth, whereas C alloying typically induces a random nanostructure consisting of a narrow size distribution of 1-nm-sized objects with a high density, consistent with the notably poorer opto-electronic behavior of these alloys.

14. SUBJECT TERMS

amorphous silicon ; microstructure ; small-angle X-ray scattering ; photovoltaics ; solar cells

15. NUMBER OF PAGES

40

16. PRICE CODE

17. SECURITY CLASSIFICATION OF REPORT	18. SECURITY CLASSIFICATION OF THIS PAGE	19. SECURITY CLASSIFICATION OF ABSTRACT	20. LIMITATION OF ABSTRACT
Unclassified	Unclassified	Unclassified	UL